

# A Torsional potential for graphene derived from fitting to DFT results

Georgios D. Chatzidakis

*Department of Physics, National Technical University of Athens, GR-15780 Athens, Greece*

George Kalosakas

*Materials Science Department, University of Patras, Rio GR-26504, Greece and  
Crete Center for Quantum Complexity and Nanotechnology (CCQCN),  
Physics Department, University of Crete GR-71003 Heraklion, Greece*

Zacharias G. Fthenakis

*Institute of Electronic Structure and Laser, FORTH, Heraklion, Greece and  
Department of Physics, University of South Florida, Tampa, Florida 33620, USA*

Nektarios N. Lathiotakis

*Theoretical and Physical Chemistry Institute, National Hellenic Research Foundation,  
Vass. Constantinou 48, GR-11635 Athens, Greece*

(Dated: September 14, 2021)

We present a simple torsional potential for graphene to accurately describe its out-of-plane deformations. The parameters of the potential are derived through appropriate fitting with suitable DFT calculations regarding the deformation energy of graphene sheets folded around two different folding axes, along an armchair or along a zig-zag direction. Removing the energetic contribution of bending angles, using a previously introduced angle bending potential, we isolate the purely torsional deformation energy, which is then fitted to simple torsional force fields. The presented out-of-plane torsional potential can accurately fit the deformation energy for relatively large torsional angles up to 0.5 rad. To test our proposed potential, we apply it to the problem of the vertical displacement of a single carbon atom out of the graphene plane and compare the obtained deformation energy with corresponding DFT calculations. The dependence of the deformation energy on the vertical displacement of the pulled carbon atom is indistinguishable in these two cases, for displacements up to about 0.5 Å. The presented potential is applicable to other  $sp^2$  carbon structures.

## I. INTRODUCTION

Following the isolation of single layer graphene [1] an enormous research effort has been devoted to the study of this two-dimensional material and its properties [2–5]. Potential applications have been explored in electronics [6], opto-electronics [7], gas filtering [8], energy storage [9], uses related to its unique mechanical properties [10–12], etc.

Many empirical force fields have been used in atomistic simulations, calculating various structural, mechanical or phonon properties of graphene [13–23]. Besides the older, well known Tersoff [24, 25] and Brenner [26] potentials, more accurate force fields have been introduced the last two decades. For example, optimized parameter sets for the latter potentials, providing better description of structural and phonon properties of graphene are presented in Ref. [27]. LCBOP [28, 29] and AIREBO [30] are efficient potentials that have been widely applied in many calculations. Other potentials leading to good predictions of elastic and thermal properties of graphene have been also discussed [31].

More recently, we have presented simple analytical expressions for the accurate description of bond stretching and angle bending potentials of graphene [12]. These potentials are derived by fitting analytical functions to the deformation energy of proper distortions of graphene,

obtained through accurate calculations from first principles' methods (DFT). The presented force field is applicable only to distortions restricted within the plane of graphene. These in-plane potentials can accurately describe elastic properties and the mechanical response of graphene in various extensional loads [12]. In this work, using similar ideas and methods, we extend this force field with torsional energy terms, in order to be able to describe out-of-plane distortions in graphene. The basic motivation is to provide a simple and computational efficient classical potential which can be used for accurate large-scale atomistic calculations. The torsional potential presented here is also capable to describe other non-planar  $sp^2$  carbon systems, like fullerenes and carbon nanotubes [32].

In the present work, we describe in detail the procedure followed and the necessary analytical calculations in order to fit the proposed torsional potential to ab-initio data. The full potential is then tested in the case of the deformation energy due to the vertical displacement of a C atom outside graphene's plane. A more comprehensive benchmark study for fullerenes, nanotubes and graphene's phonons is presented elsewhere [32]. We have considered two types of folding of graphene sheets around different axes (either an armchair or a zig-zag one). The corresponding deformation energies are calculated using DFT methods. Following the removal of the contribution

arXiv:1707.09059v1 [cond-mat.mtrl-sci] 27 Jul 2017

of angle bending terms in the total deformation energy, we isolated the pure torsional energy. Then, the analytic modeling of this energy in terms of individual torsional contributions, leads to a fitting procedure providing the optimal parameters of the out-of-plane torsional energy.

This paper is organized as follows: In Sect. II we describe the structures and methodology adopted for the DFT simulations that was used to obtain the deformation energies. Then in Sect. III, we present the analytic work for removing the angle bending contributions from the deformation energies. The analytic expressions of the torsional energy terms in terms of the folding angles are provided in Sec. IV. The fitting of the torsional terms of both Model 1 and 2 is described in Sec. V completing the presentation of the derivation of the new torsional force fields. Then, in Sec. VI, we present a test case, the deformation energy due to the vertical displacement of a carbon atom outside graphene’s plane, as a first application of the proposed scheme and compare the prediction of Models 1 and 2 with DFT results. Finally, a summary and conclusions are given in Sect. VII.

## II. STRUCTURES AND DFT CALCULATIONS

### A. Torsion angles in graphene

In Fig. 1, we show a part of the honeycomb structure of graphene and a few carbon-atom positions labeled as  $i$ ,  $j$ ,  $k$ ,  $l$ ,  $m$ . The quadruple  $(i, j, k, l)$ , with 3 of these positions belonging to the same hexagonal ring and one to an adjacent is customary called “trans” while the quadruple  $(i, j, k, m)$ , with all belonging to the same ring, “cis”. In the case that the structure is distorted and the atoms in the quadruple are no longer co-planar, we can define a torsion angle, which we label as  $(i-j-k-l)$ , as the dihedral angle of the planes  $i-j-k$ ,  $j-k-l$ . The torsion angles can then be classified as “trans” or “cis” accordingly. The dihedral angle between two planes, e.g.  $i-j-k$  and  $j-k-l$  can be defined as the angle between the vectors perpendicular to the planes. We assumed that the perpendicular vectors are pointing inwards for clockwise triples (like  $i-j-k$ ) or outwards for anti-clockwise triples (like  $j-k-l$ ). Under this assumption, torsional angles are in the range  $[0, \pi]$  with “cis” angles smaller than  $\pi/2$  and “trans” angles larger than  $\pi/2$ .

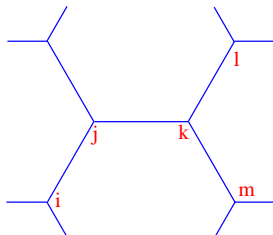


FIG. 1: Graphene’s honeycomb lattice with a few atomic positions labeled as  $i$ ,  $j$ ,  $k$ ,  $l$ .

### B. DFT results

DFT calculations were performed for two distorted graphene structures, one that graphene is folded around an armchair axis and one around a zig-zag. These structures are shown in Fig. 2 where we label all atoms relevant to the present discussion. They are periodic along the folding axis while on the vertical they are not. The folding angle around either the armchair or zig-zag axis is denoted by  $\phi$ . With symbol  $\theta$ , we denote “usual” angles between carbon bonds (bending angles) and with  $\omega$  torsion angles as defined in the previous subsection.

All calculations were performed with Quantum-Espresso periodic-DFT code [33], with the same pseudopotential [34] as in Ref. 12. The wave-function and density plane-wave cutoffs were chosen 40 Ry and 400 Ry respectively. The unit cell we chose is minimal in the periodic direction (that of the folding axis) while, in the vertical, it is appropriately large to avoid edge-effects. Thus, the simulated structures are nanoribbons that are folded around their middle line direction. In the case of the armchair folding (Fig. 2(top)), the vertical unit cell direction is such that neighbors up to the 5th in the vertical direction were included. In the case of the zig-zag folding that size is long enough to include up to 8th neighbors. Thus, the unit cells contain 22 and 18 atoms for the armchair and the zig-zag folding, respectively. In the reciprocal space, we used a mesh of  $1 \times 24 \times 1$ , i.e. 24 points were assumed along the bending direction that the structure is periodic.

In Fig. 3, we show with filled circles the total deformation energy per unit cell along the folding direction, as calculated by DFT, as a function of the folding angle  $\phi$ , for both armchair and zig-zag folding actions,  $E_d^{(a)}$  and  $E_d^{(z)}$ , respectively. The total deformation energy per unit-cell is taken as the energy difference between the folded structure and the not folded one ( $\phi = 0$ ). Apparently, the two structure distortions due to the considered foldings are complex and consist of several individual angle-bending and torsional deformations. Note that bond lengths are not altered so there is no bond-stretching contribution in the total deformation energy. As we see in Fig. 3, the contribution from angle bending is significant for  $\phi$  larger than 0.2 rad. In order to perform a fitting for the torsional terms alone, we first need to exclude angle-bending contributions from the total deformation energy. In order to do so, (i) we identify all angle-bending terms and express analytically their corresponding bending angles  $\theta$  in terms of  $\phi$  and then (ii) we remove the angle-bending terms using the analytic terms in the Ref. [12]. The residual, torsional energy per unit cell, when the contribution from angle-bending is subtracted, as a function of the out-of-plane folding angle  $\phi$  is shown in Fig. 3 (diamonds), for the two folding directions. In order to fit an analytic expression to the torsional terms, we also have to (i) identify all the individual torsional terms that contribute for each of the

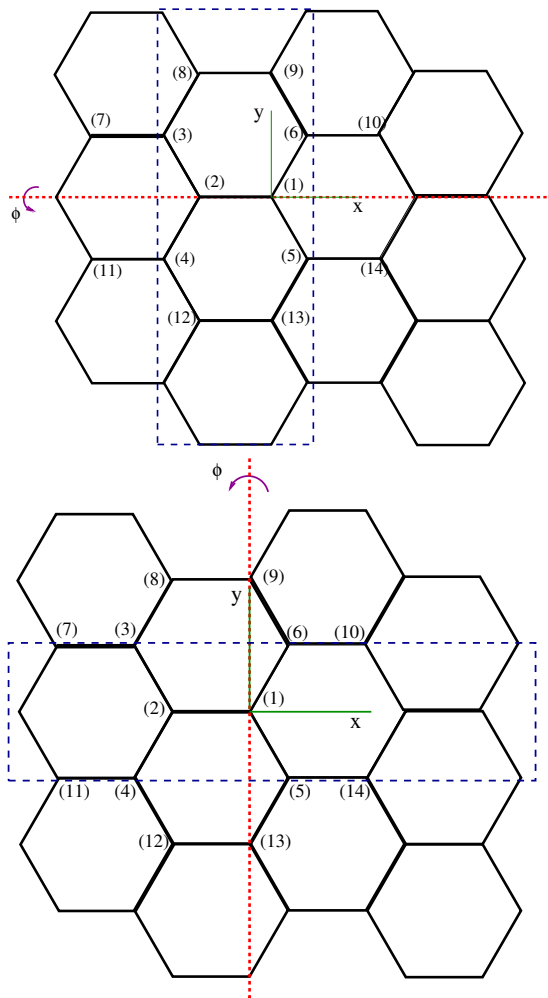


FIG. 2: Part of graphene's structure with the armchair (top) and zig-zag (bottom) folding axes. We label several atoms that are mentioned in the text. The structure is periodic along the bending axis direction and part of the unit cell is shown in dashed blue line. The actual size of the unit cell along the direction vertical to the folding axis adopted in the DFT calculations is described in the text.

zig-zag and armchair cases, and subsequently (ii) express the corresponding torsion angles as functions of the folding angle,  $\phi$ . These steps are described below where we provide all necessary analytical expressions.

### III. REMOVING THE ANGLE-BENDING TERMS

#### A. For the folding around armchair axis

The folding around the armchair direction (Fig. 2, top) alters two bond angles per unit cell,  $(3\hat{2}4)$ ,  $(6\hat{1}5)$ , which are equal. One can show that these angles, in terms of

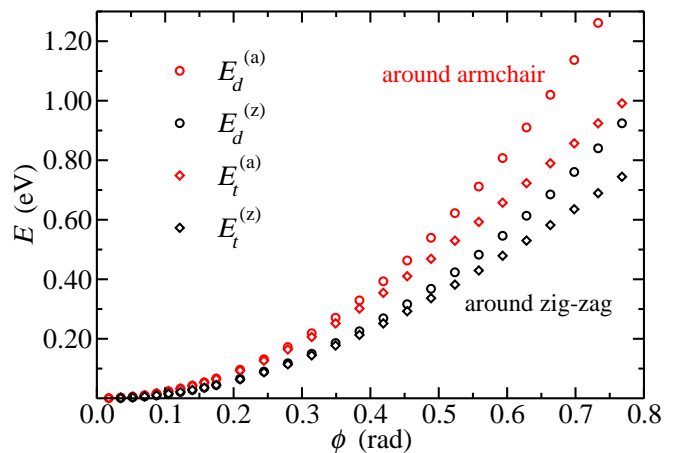


FIG. 3: The total deformation energies,  $E_d^{(a)}$ ,  $E_d^{(z)}$ , calculated with DFT and the total torsional energies,  $E_t^{(a)}$ ,  $E_t^{(z)}$ , after removing angle bending terms, as a function of the folding angle  $\phi$ . The indices (a), (z) correspond to the armchair (red) and zig-zag (black) folding cases, respectively.

$\phi$ , are given by

$$\theta^{(a)} = 2 \arcsin \left( \sqrt{\frac{3}{8}} \sqrt{\cos \phi + 1} \right) \quad (1)$$

The angle-bending energy that one needs to remove from the total energy is

$$U_b^{(a)} = 2V_b(\theta^{(a)}(\phi)), \quad (2)$$

where  $V_b(\theta)$  is the analytical expression for the angle bending given in Ref. [12], i.e.

$$V_b(\theta) = \frac{k}{2} \left( \theta - \frac{2\pi}{3} \right)^2 - \frac{k'}{3} \left( \theta - \frac{2\pi}{3} \right)^3, \quad (3)$$

with  $k = 7.0 \text{ eV/rad}^2$  and  $k' = 4 \text{ eV/rad}^3$ .

Removing these terms from the total deformation energies,  $E_d^{(a)}$  we find the total torsional energy

$$E_t^{(a)} = E_d^{(a)} - U_b^{(a)}, \quad (4)$$

shown in Fig. 3.

#### B. For the folding around zig-zag axis

Similarly, the folding around the zig-zag direction (Fig. 2, (bottom)) affects two angles per unit cell,  $(2\hat{1}6)$ ,  $(2\hat{1}5)$ , that are also equal. In terms of  $\phi$ , these angles are given by

$$\theta^{(z)} = 2 \arcsin \left( \frac{1}{2} \sqrt{2 + \cos \phi} \right) \quad (5)$$

Again, the angle-bending energy that one needs to remove from the total energy is

$$U_b^{(z)} = 2V_b(\theta^{(z)}(\phi)), \quad (6)$$

we remove these terms from the total deformation energy and we find the total torsional energy,

$$E_t^{(z)} = E_d^{(z)} - U_b^{(z)}, \quad (7)$$

shown in Fig. 3.

#### IV. ANALYTICAL EXPRESSIONS FOR THE TORSIONAL TERMS

Here we provide analytical expressions,  $U_t^{(a)}(\phi)$ ,  $U_t^{(z)}(\phi)$ , for the total torsional energies, as functions of  $\phi$  that will contain parameters to be fitted so that these expressions reproduce as close as possible the  $E_t^{(a)}$ ,  $E_t^{(z)}$  points shown in Fig. 3. To arrive to such analytical expressions we need first to identify all altered torsion angles (per unit cell) and express them in terms of the folding angle  $\phi$ . Then,  $U_t^{(a)}(\phi)$ ,  $U_t^{(z)}(\phi)$  will be just the sum of all individual torsional terms that correspond to these altered torsional angles.

Regarding the individual torsional energy term,  $V_t(\omega)$ , two different functional forms would be considered. The most frequently used formula, referred as Model 1 here, is

$$V_t(\omega) = \frac{1}{2}V_1 [1 + \cos\omega] + \frac{1}{2}V_2 [1 - \cos(2\omega)]. \quad (8)$$

An alternative model that we considered, which we call Model 2, assumes a different fitting formula for cis or trans dihedral angles  $\omega$

$$\begin{aligned} V_t^{(\text{cis})}(\omega) &= K_{\text{cis}} [1 - \cos(2\omega)], \\ V_t^{(\text{trans})}(\omega) &= K_{\text{trans}} [1 - \cos(2\omega)], \end{aligned} \quad (9)$$

where either the first or the second expression is used for cis or trans torsion angles, respectively. Below we use both Models 1 and 2 to fit their parameters to the obtained DFT results.

##### A. For the folding around armchair axis

Inspecting the Fig. 2 (top) we identify the following torsion (dihedral) angles per unit cell that are altered by folding along the armchair axis

- 2 trans dihedral angles, (5-1-2-3), (4-2-1-6), with

$$\omega_1^{(a)}(\phi) = \arccos(-\cos\phi) \quad (10)$$

- 4 cis dihedral angles, (11-4-2-3), (14-5-1-6), (7-3-2-4), (10-6-1-5), with

$$\omega_2^{(a)}(\phi) = \arccos\left(\sqrt{3}\frac{1 + \cos\phi}{\sqrt{9\sin^2\phi + 6(1 + \cos\phi)}}\right) \quad (11)$$

- 4 trans dihedral angles, (12-4-2-3), (13-5-1-6), (8-3-2-4), (9-6-1-5), with

$$\omega_3^{(a)}(\phi) = \arccos\left(-\sqrt{3}\frac{1 + \cos\phi}{\sqrt{9\sin^2\phi + 6(1 + \cos\phi)}}\right) \quad (12)$$

Through the angle expressions given above, the total torsional energy,  $U_t^{(a)}$  within the Model 1, becomes an analytic function of  $\phi$ :

$$\begin{aligned} U_t^{(a)}(\phi) &= 2V_t(\omega_1^{(a)}(\phi)) + 4V_t(\omega_2^{(a)}(\phi)) \\ &\quad + 4V_t(\omega_3^{(a)}(\phi)) \end{aligned} \quad (13)$$

where  $V_t(\omega)$  is the individual torsional term Eq. (8).

For the Model 2, the corresponding expression of the total torsional energy  $U_t^{(a)}$  is

$$\begin{aligned} U_t^{(a)}(\phi) &= 2V_t^{(\text{trans})}(\omega_1^{(a)}(\phi)) + 4V_t^{(\text{cis})}(\omega_2^{(a)}(\phi)) \\ &\quad + 4V_t^{(\text{trans})}(\omega_3^{(a)}(\phi)) \end{aligned} \quad (14)$$

with  $V_t^{(\text{cis})}$  and  $V_t^{(\text{trans})}$  given by Eq. (9).

##### B. For the folding around zig-zag axis

Inspecting the Fig. 2 (bottom) we identify the following dihedral angles per unit cell that are affected

- 2 cis dihedral angles, (3-2-1-6), (4-2-1-5), with

$$\omega_1^{(z)}(\phi) = \arccos\left(\sqrt{\frac{3}{\sin^2\phi + 3}}\right) \quad (15)$$

- 2 trans dihedral angles, (4-2-1-6), (3-2-1-5), with

$$\omega_2^{(z)}(\phi) = \arccos\left(-\sqrt{\frac{3}{\sin^2\phi + 3}}\right) \quad (16)$$

- 2 cis dihedral angles, (2-1-5-13), (2-1-6-9), with

$$\omega_3^{(z)}(\phi) = \arccos\left(\sqrt{\frac{3}{\sin^2\phi + 3}}\cos\phi\right) \quad (17)$$

- 2 trans dihedral angles, (2-1-5-14), (2-1-6-10), with

$$\omega_4^{(z)}(\phi) = \arccos\left(-\sqrt{\frac{3}{\sin^2\phi + 3}} \cos\phi\right) \quad (18)$$

And the total torsional energy is given by

$$U_t^{(z)}(\phi) = 2V_t(\omega_1^{(z)}(\phi)) + 2V_t(\omega_2^{(z)}(\phi)) + 2V_t(\omega_3^{(z)}(\phi)) + 2V_t(\omega_4^{(z)}(\phi)), \quad (19)$$

where  $V_t$  is given by Eq. (8) for Model 1. In case of Model 2, the above formula becomes

$$U_t^{(z)}(\phi) = 2V_t^{(\text{cis})}(\omega_1^{(z)}(\phi)) + 2V_t^{(\text{trans})}(\omega_2^{(z)}(\phi)) + 2V_t^{(\text{cis})}(\omega_3^{(z)}(\phi)) + 2V_t^{(\text{trans})}(\omega_4^{(z)}(\phi)). \quad (20)$$

## V. FITTING PROCEDURE

The total torsional energy data,  $(\phi_i, E_{t,i}^{(a)})$  and  $(\phi_i, E_{t,i}^{(z)})$ , shown in red and black diamonds in the Fig. 3, and the analytical (to be fitted) expressions  $U_t^{(a)}$ ,  $U_t^{(z)}$  given in the Eqs. (13) and (19) for the Model 1 (or the Eqs. (14) and (20) for the Model 2) can be used to obtain the optimal parameters  $V_1$  and  $V_2$  (or  $K_{\text{cis}}$  and  $K_{\text{trans}}$ ) of the individual torsional terms so that  $U_t^{(a)}$ ,  $U_t^{(z)}$  reproduce the dependence of  $E_t^{(a)}(\phi)$  and  $E_t^{(z)}(\phi)$  as close as possible. For this purpose, adopting a standard procedure, we minimize an objective function  $O(V_1, V_2)$  which is the equal-weighted sum of the square differences,

$$O(V_1, V_2) = \sum_{i=1}^{\phi_i < \phi_{\text{max}}} \left[ E_{t,i}^{(a)} - U_t^{(a)}(\phi_i) \right]^2 + \sum_{i=1}^{\phi_i < \phi_{\text{max}}} \left[ E_{t,i}^{(z)} - U_t^{(z)}(\phi_i) \right]^2. \quad (21)$$

The sums in the above expression runs over all  $i$  for which  $\phi_i$  is smaller than an upper-limit angle  $\phi_{\text{max}}$ .

For the Model 1, the fitted total torsional energies  $U_t^{(a)}(\phi)$  and  $U_t^{(z)}(\phi)$  given in the Eqs. (13) and (19) depend on  $V_1$  and  $V_2$  through the dependence of the individual terms  $V_t$  of the Eq. (8).

In the case of Model 2, we are optimizing  $K_{\text{cis}}$  and  $K_{\text{trans}}$  parameters, and the expressions (14) and (20) are used instead and the individual terms  $V_t$  are given by the Eq. (9).

The choice of  $\phi_{\text{max}}$  is expected to affect the quality of fitting for small and large  $\phi$ . We are interested in seeing whether the fitting parameters depend on  $\phi_{\text{max}}$  and, if so, at what extend.

## A. Model 1: fitting Results for $V_1, V_2$

We performed fitting of  $V_1, V_2$  of Eq. (8), for three different  $\phi_{\text{max}}$  values:  $10^\circ$ ,  $20^\circ$  and  $30^\circ$ . The optimal parameters  $V_1$  and  $V_2$  given in table I.

$\phi_{\text{max}}$	$V_1$ (eV)	$V_2$ (eV)
10	-0.00013	0.221
20	-0.00017	0.226
30	-0.00035	0.233

TABLE I: **Model 1:** Optimal fitting parameters  $V_1$  and  $V_2$  for Model 1, for the three different values of  $\phi_{\text{max}}$  examined.

In Fig. 4, we show, the total torsional energies,  $E_t^{(a)}$  and  $E_t^{(z)}$  and the fitted lines for these three values of  $\phi_{\text{max}}$ . As we see, the fitting is better for small values of  $\phi$  and deteriorates as  $\phi$  increases. In all cases, it reproduces the armchair data in closer agreement than the zig-zag, i.e. for a larger range of  $\phi$ . For  $\phi_{\text{max}} = 10^\circ$ , there is a satisfactory agreement for values of  $\phi$  up to 0.55 rad for the armchair case and 0.4 rad for the zig-zag case. For  $\phi_{\text{max}} = 20^\circ$ , the range of satisfactory agreement increases roughly up to 0.65 rad and 0.45 rad for the armchair and zig-zag cases respectively. Finally for  $\phi_{\text{max}} = 30^\circ$ , the agreement range increases further up to 0.7 rad and 0.5 rad, respectively. Although by increasing  $\phi_{\text{max}}$ , the range of satisfactory agreement also increases, this is at the cost of the agreement for smaller angles. As the code is trying to fit better at larger values of  $\phi$  the quality for smaller angles deteriorates. This deterioration, however, is rather small as we observe in the insets of the Figs. 4(a), (b), (c) where we zoom in that region.

However, in general, for angles  $\phi$  up to 0.4 rad ( $22^\circ$ ) corresponding to energies 0.2 to 0.3 eV, all fittings are satisfactory. On the other hand, as we see in Table I, the fitted values of  $V_1$  and  $V_2$  are not so sensitive to the value of  $\phi_{\text{max}}$ :  $V_1$  remains close to 0 while  $V_2$  is in the range 0.22-0.23 eV. In addition, the large value of  $V_2$ , i.e. 0.23 eV, obtained for  $\phi_{\text{max}} = 20^\circ, 30^\circ$  performs better for larger angles, up to 0.5 rad ( $\sim 30^\circ$ ), corresponding to energies of 0.4-0.5 eV, while on the other hand the fitted results in the region of small  $\phi$  remain satisfactory. These considerations suggest that it is quite reasonable to adopt as optimal  $V_1 = 0$  and  $V_2 = 0.23$  eV and our proposed torsional potential has the simple form

$$V_t(\omega) = \frac{1}{2}V_2(1 - \cos(2\omega)), \quad V_2 = 0.23 \text{ eV}. \quad (22)$$

This potential is shown in Fig. 5 together with  $E_t^{(a)}$  and  $E_t^{(z)}$ .

## B. Model 2: fitting results for $K_{\text{cis}}, K_{\text{trans}}$

As in the previous section, we performed the fitting of  $K_{\text{cis}}$  and  $K_{\text{trans}}$  of Eq. (9) for the same values of  $\phi_{\text{max}}$ ,

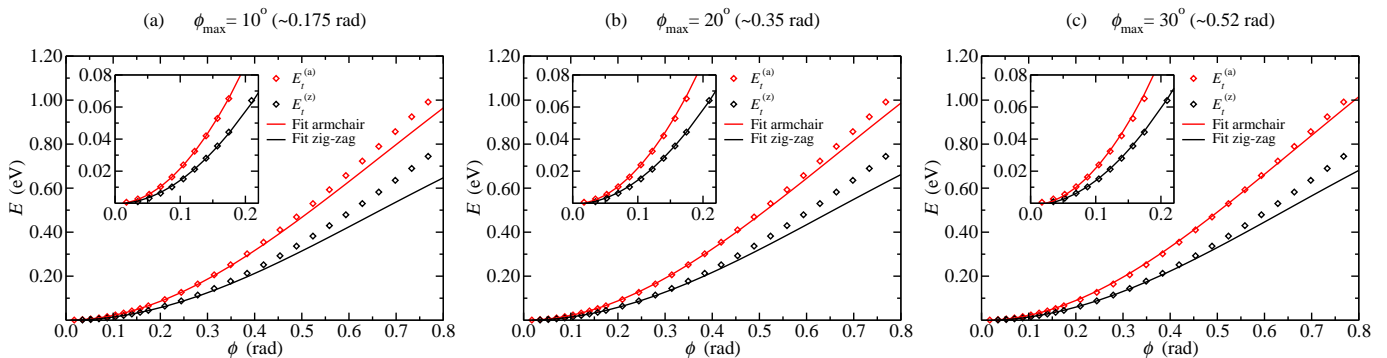


FIG. 4: **Model 1:** Fit of the analytical expressions with the numerically derived data  $E_t^{(a)}$  and  $E_t^{(z)}$  of the total torsional energy, for different choices of  $\phi_{\max}$  equal to (a)  $10^\circ$ , (b)  $20^\circ$ , and (c)  $30^\circ$ . In the inset we zoom in the region of small angles  $\phi$ .

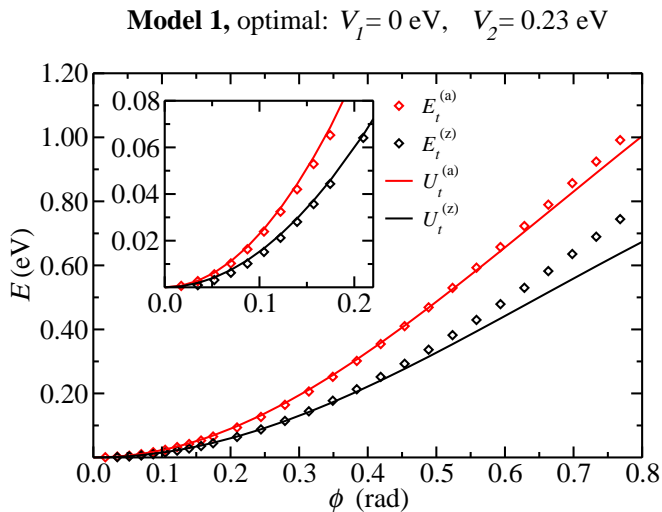


FIG. 5: The analytical torsional energies considering Model 1, for the folding around the armchair (a) and zig-zag (z) axes,  $U_t^{(a)}$  and  $U_t^{(z)}$ , Eqs. (13) and (19) respectively, using the proposed parameters  $V_1 = 0$  eV and  $V_2 = 0.23$  eV (lines), compared to the numerically derived data  $E_t^{(a)}$  and  $E_t^{(z)}$  (points). The inset zooms in small values of  $\phi$  to illustrate the quality of the fit in that region.

i.e.  $10^\circ$ ,  $20^\circ$  and  $30^\circ$ . The optimal parameters  $K_{\text{cis}}$  and  $K_{\text{trans}}$  for each of these cases are given in Table II. In Fig. 6, we show the fitting lines for the armchair and zig-zag folding cases for all three values of  $\phi_{\max}$  compared to the data points for the total torsional energy per unit cell,  $E_t^{(a)}$  and  $E_t^{(z)}$ . The fitting quality is quite similar to that of the previous section. Again, for  $\phi_{\max} = 20^\circ$  and  $30^\circ$ , the quality improves for larger values of  $\phi$  and at the same time the fit for smaller  $\phi$  does not deteriorate substantially. Thus, we propose a rounded optimal set  $K_{\text{cis}} = 0.14$  eV and  $K_{\text{trans}} = 0.10$  eV which is close to the values obtained for  $\phi_{\max} = 20^\circ$  and  $30^\circ$ . In Fig. 7, we show the torsional energy obtained with Model 2 and these values for  $K_{\text{cis}}$  and  $K_{\text{trans}}$  compared with the data  $E_t^{(a)}$  and  $E_t^{(z)}$ .

$\phi_{\max}$	$K_{\text{cis}}$ (eV)	$K_{\text{trans}}$ (eV)
10	0.104	0.112
20	0.134	0.096
30	0.150	0.090

TABLE II: **Model 2:** Optimal fitting parameters  $K_{\text{cis}}$  and  $K_{\text{trans}}$ , for the three different values of  $\phi_{\max}$  examined.

To summarize, for the Model 2, we propose

$$\begin{aligned} V_t^{(\text{cis})}(\omega) &= K_{\text{cis}} [1 - \cos(2\omega)], & K_{\text{cis}} &= 0.14 \text{ eV}, \\ V_t^{(\text{trans})}(\omega) &= K_{\text{trans}} [1 - \cos(2\omega)], & K_{\text{trans}} &= 0.1 \text{ eV}, \end{aligned} \quad (23)$$

where either the first or the second expression is used depending on whether the torsional angle  $\omega$  is cis or trans.

### C. Comparison of the two models

In Fig. 8 we show the torsional energies per unit cell, for both fitting forms of Models 1 and 2, for the case of the optimal parameters we arrived at. We notice that the two models are of the same quality. They almost coincide for the armchair case, while for the zig-zag, the Model 2 is slightly better for larger  $\phi$ 's and the Model 1 marginally better for smaller. The differences however are not significant for  $\phi$ 's up to 0.5 rad.

Note that the obtained optimal parameters of Model 2,  $K_{\text{cis}} = 0.14$  eV and  $K_{\text{trans}} = 0.10$  eV, are close to each other, indicating that a single parameter with value the average of them would offer a reasonable description. Moreover, this average value is almost equal to  $V_2/2$ . Thus, it is rather unnecessary to assume different parameters for *cis* and *trans* dihedral angles and, to keep things as simple as possible, the simple form of the Eq. (22), is quite sufficient to describe all torsional distortions. Therefore, the Model 1 of Eq. (22) is our proposed one, containing a single parameter  $V_2$ . We should mention that our modeling describes accurately the energy of torsional angles  $\phi$  up to 0.5 rad which is already a sufficiently large value, corresponding to rather unphysical structural deformations.

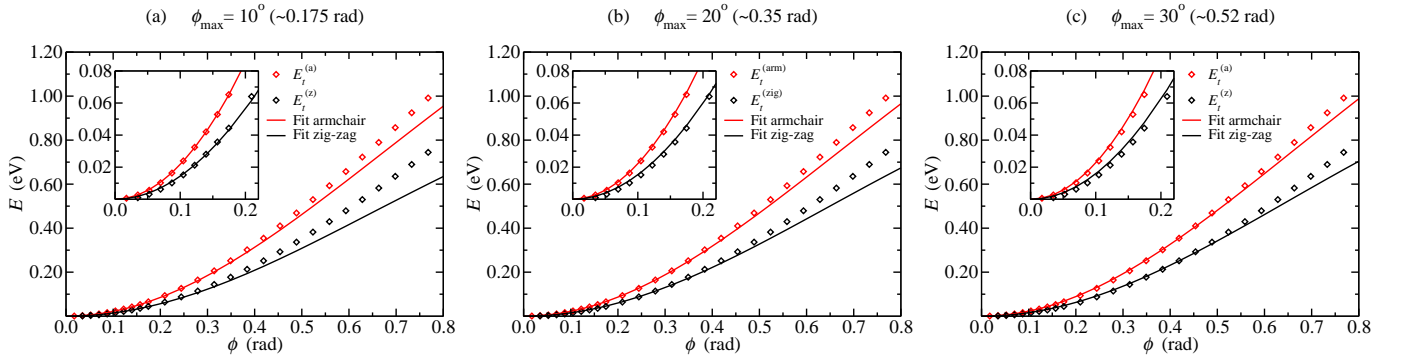


FIG. 6: **Model 2:** Fit of the analytical expressions with the numerically derived data  $E_t^{(a)}$  and  $E_t^{(z)}$  of the total torsional energy, for different choices of  $\phi_{\max}$  equal to (a)  $10^\circ$ , (b)  $20^\circ$ , and (c)  $30^\circ$ . In the inset we zoom in the region of small angles  $\phi$ .

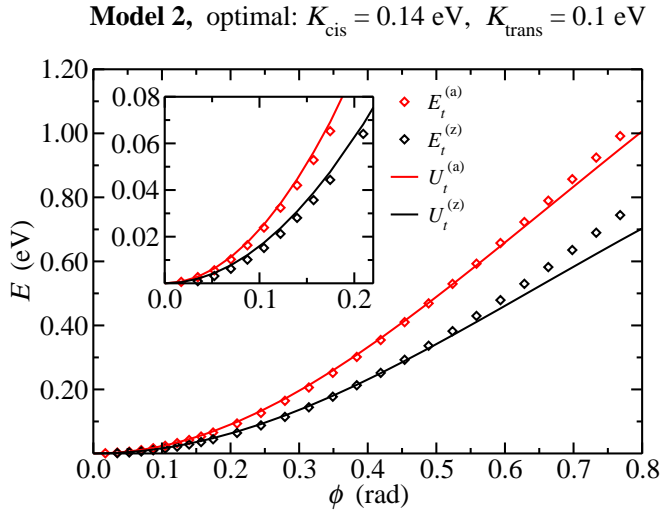


FIG. 7: The analytical torsional energies considering Model 2, for the folding around the armchair (a) and zig-zag (z) axes,  $U_t^{(a)}$  and  $U_t^{(z)}$ , Eqs. (14) and (20) respectively, using the proposed parameters  $K_{\text{cis}}=0.14$  eV,  $K_{\text{trans}}=0.10$  eV, compared to the data  $E_t^{(a)}$  and  $E_t^{(z)}$ . The inset zooms in small values of  $\phi$  to illustrate the quality of the fit in that region.

## VI. APPLICATION TO THE VERTICAL DISPLACEMENT OF A CARBON ATOM IN GRAPHENE

In order to test the accuracy of the proposed parameters for the torsional terms, we consider the deformation energy of graphene due to a vertical, out-of-plane displacement of a single carbon atom. We consider that apart from the vertically displaced atom, all other atoms remain fixed at their equilibrium positions within graphene's plane. The task is to compare the deformation energy obtained by the present potential, along with the in-plane force field of Ref. [12], with that obtained by DFT calculations (using the same method that was used to produce the data discussed above).

The process of moving a carbon atom vertically outside

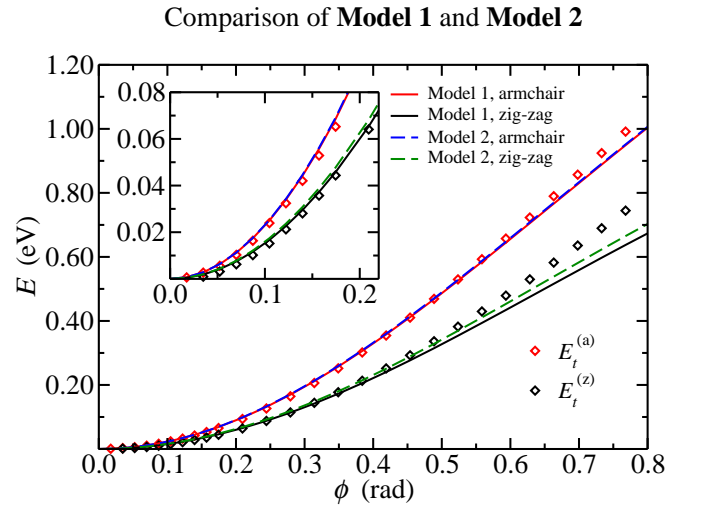


FIG. 8: Comparison between the fitting of the two models: Model 1 with values  $V_1=0$  eV,  $V_2=0.23$  eV and Model 2 with values  $K_{\text{cis}}=0.14$  eV,  $K_{\text{trans}}=0.10$  eV.

graphene's plane is described by a deformation energy consisting of all kinds of individual terms, i.e. bond-stretching, angle-bending and of course torsional terms.

Concerning the bond-stretching terms, the vertical movement of a carbon atom at a displacement  $z$  over the plane, alters only the three bonds of that atom (see Fig. 9). If the length of these bonds at  $z=0$  is  $d$  their altered length  $d'$  becomes

$$d'(z) = \sqrt{d^2 + z^2} \quad (24)$$

At the same time, two different kinds of angle-bending terms appear corresponding to: (i) the three angles,  $\theta_1$ , between the atom's bonds (marked in red in Fig. 9) and (ii) the six angles,  $\theta_2$  between these bonds and the bonds marked in blue in Fig. 9. These angles can be expressed in terms of the displacement  $z$  as

$$\theta_1(z) = \arccos\left(\frac{2z^2 - d^2}{2(d^2 + z^2)}\right) \quad (25)$$

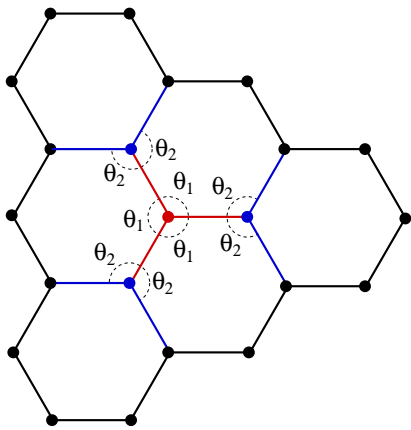


FIG. 9: A vertical displacement (normal to the page) of a C atom (marked red) results in contributions to the total deformation energy from bond-stretching (elongation of red bonds), angle-bending (altering  $\theta_1$  and  $\theta_2$  angles), and torsional terms (twisting around red and blue bonds).

and

$$\theta_2(z) = \arccos\left(-\frac{d}{2\sqrt{d^2+z^2}}\right) \quad (26)$$

Finally, several torsional terms also contribute. There are rotations around the 3 bonds of the displaced atom and its first neighbors (marked in red in Fig. 9) as well as rotations around the 6 bonds of the first neighbors and the second neighbors. These rotations correspond to the following torsional angles

- 6 cis dihedral angles around the bonds marked in red in Fig. 9 given by

$$\omega_{\text{cis}}^{(1)}(z) = \arccos\left(\frac{\frac{3}{4}}{\sqrt{\left(\frac{z}{d}\right)^2 + \frac{3}{4}}}\right) \quad (27)$$

- 6 trans dihedral angles around the bonds marked in red in Fig. 9 given by

$$\omega_{\text{trans}}^{(1)}(z) = \arccos\left(\frac{-\frac{3}{2}\left(\frac{z}{d}\right)^2 - \frac{3}{4}}{\sqrt{\left(\frac{z}{d}\right)^2 + \frac{3}{4}}}\right) \quad (28)$$

- 6 cis dihedral angles around the bonds marked in blue in Fig. 9 given by

$$\omega_{\text{cis}}^{(2)}(z) = \arccos\left(\frac{1}{\sqrt{\frac{4}{3}\left(\frac{z}{d}\right)^2 + 1}}\right) \quad (29)$$

- 6 trans dihedral angles around the bonds marked in blue in Fig. 9 given by

$$\omega_{\text{trans}}^{(2)}(z) = \arccos\left(\frac{-1}{\sqrt{\frac{4}{3}\left(\frac{z}{d}\right)^2 + 1}}\right) \quad (30)$$

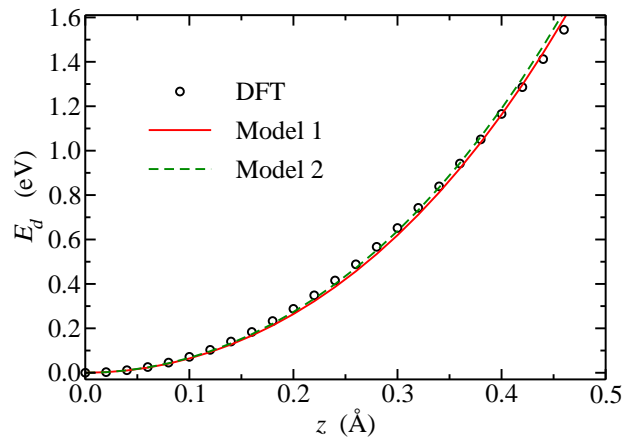


FIG. 10: The deformation energy,  $E_d$ , written in analytical form in Eq. (31), due to the vertical out-of-plane displacement of a single carbon atom in graphene as a function of the vertical displacement  $z$ , calculated with the present potential and compared to DFT results.

Then, the deformation energy is given by

$$\begin{aligned} E_d(z) = & 3V_s(d'(z)) + 3V_b(\theta_1(z)) + 6V_b(\theta_2(z)) \\ & + 6V_t(\omega_{\text{cis}}^{(1)}(z)) + 6V_t(\omega_{\text{trans}}^{(1)}(z)) \\ & + 6V_t(\omega_{\text{cis}}^{(2)}(z)) + 6V_t(\omega_{\text{trans}}^{(2)}(z)), \end{aligned} \quad (31)$$

where  $V_s(d)$ ,  $V_b(\theta)$  are respectively the bond stretching and angle bending terms given in Ref. [12].  $V_t$  is the individual torsional term of Eq. (22) for Model 1, while for Model 2 it should be replaced by  $V_t^{(\text{cis})}$  or  $V_t^{(\text{trans})}$  of Eq. (23) for the two  $\omega_{\text{cis}}$  and the two  $\omega_{\text{trans}}$  respectively. In Eq. (31), the deformation energy,  $E_d$ , becomes an analytic function of  $z$  through the explicit dependence on  $z$  of the bonds  $d'$ , the angles  $\theta_1$ ,  $\theta_2$  and the dihedral angles  $\omega_{\text{cis}}^{(1)}$ ,  $\omega_{\text{trans}}^{(1)}$ ,  $\omega_{\text{cis}}^{(2)}$ ,  $\omega_{\text{trans}}^{(2)}$ .

In Fig. 10, we show  $E_d$  in comparison with the corresponding DFT results. As we see, both models perform equally well and the error does not exceed 0.05 eV for the deformation range shown. There are small differences in their agreement with DFT, for example Model 2 seems slightly better for intermediate-size displacements while Model 1 for larger ones, however, these small differences are insignificant validating our preference for Model 1 on the basis of its simplicity.

## VII. CONCLUSION

In summary, we present a simple torsional force field for graphene and other  $\text{sp}^2$  carbon nanostructures. To obtain this potential we performed two sets of DFT calculations by folding two different graphene nanoribbon structures around their middle line. The first set of calculations concern the folding of an armchair nanoribbon around its middle line, an armchair direction. The second concerns the folding of a zig-zag nanoribbon around



its middle line which is a zig-zag direction. From the deformation energies we isolated the “pure” torsional contribution by removing angle bending terms with the use of our previously proposed angle bending terms[12]. The purified torsional deformation energy was then fit two different analytic forms with two parameters each that we call Models 1 and 2. The first (Model 1) is that of Eq. (8) and does not distinguish torsional angles, while the second (Model 2) of Eq. (9) treats differently “cis” and “trans” torsional angles. We found that the form of Model 1 reduces to one parameter form, see Eq. (22), which was found to be an average of the “cis” and “trans” terms of Model 2 which differ very little from each other, see Eq. (23). That suggests that the use of two different terms is redundant and the single term of Model 1 suffices at a reasonable level of accuracy. We found that both models reproduce accurately the torsional deformation energy of graphene nanoribbons due to the folding we considered up to  $\theta_{\max}$  of the order of  $30^\circ$  ( $\approx 0.5$  rad).

As an additional validation test we considered the case of the deformation energy due to the vertical displacement of a single C atom outside of graphene’s plane. For this task we used the torsional terms of either Model 1 or 2 combined with the bond stretching and angle bending terms of Ref. 12. For all terms in this formula we pro-

vide analytic expressions in terms of the displacement  $z$ . We found that both models perform equally well in this case with errors not exceeding 0.05 eV for a relatively large range of  $z$ , up to 0.4-0.5 Å. The good performance of both Models in this case validates our choice for the simpler Model 1.

The torsional force field presented here, in combination with the bond stretching and angle bending terms of Ref. 12, which were also fitted to DFT results using the same density functional approximation provide a complete, accurate, but simple in form atomistic potential, which is computationally efficient due to its simplicity. Thus, we expect that it will be proven a very useful tool for large scale atomistic simulation of graphene and other  $sp^2$  nanostructures.

*Acknowledgements:* We acknowledge helpful discussions with E. N. Koukaras. The research leading to the present results has received funding from Thales project “GRAPHENECOMP”, co-financed by the European Union (ESF) and the Greek Ministry of Education (through program). NNL acknowledges support from the Hellenic Ministry of Education/GSRT (ESPA), through “Advanced Materials and Devices” program (MIS:5002409) and EU H2020 ETN project Enabling Excellence Grant Agreement 642742.

- 
- [1] K. S. Novoselov, A. K. Geim, S. V. Morozov, D. Jiang, Y. Zhang, S. V. Dubonos, I. V. Grigorieva, A. A. Firsov, *Science* **306**, 666 (2004).
- [2] A. H. Castro Neto, F. Guinea, N. M. R. Peres, K. S. Novoselov, A. K. Geim, *Rev. Mod. Phys.* **81**, 109 (2009).
- [3] L. Chen, Y. Hernandez, X. Feng, K. Mullen, *Angew. Chem. Int. Ed.* **51**, 7640 (2012).
- [4] A. C. Ferrari et al, *Nanoscale* **7**, 4598 (2015).
- [5] C. Daniels, A. Horning, A. Phillips, D. V. P. Massote, L. Liang, Z. Bullard, B. G. Sumpter, V. Meunier, *J. Phys.: Condens. Matter* **27**, 373002 (2015).
- [6] Y.-M. Lin, et al, *Science* **332**, 1294 (2011).
- [7] F. V. Kusmartsev, W. M. Wu, M. P. Pierpoint, K. C. Yung, in *Applied Spectroscopy and the Science of Nanomaterials*, Ed. P. Misra, Springer Singapore 2015.
- [8] K. Celebi, et al, *Science* **344**, 289 (2014).
- [9] M. F. El-Kady, Y. Shao, R. B. Kaner, *Nature Rev. Mater.* **1**, 16033 (2016).
- [10] C. Lee, X. Wei, J.W. Kysar, J. Hone, *Science* **321**, 385 (2008).
- [11] G. Tsoukleri, J. Parthenios, K. Papagelis, R. Jalil, A.C. Ferrari, A.K. Geim, K.S. Novoselov, C. Galiotis, *Small* **21**, 2397 (2009).
- [12] G. Kalosakas, N. N. Lathiotakis, C. Galiotis, K. Papagelis, *J. App. Phys.* **113**, 134307 (2013).
- [13] A. Fasolino, J. H. Los, M. I. Katsnelson, *Nature Mater.* **6**, 858 (2007).
- [14] K. V. Zakharchenko, M. I. Katsnelson, A. Fasolino, *Phys. Rev. Lett.* **102**, 046808 (2009).
- [15] P. Liu, Y. W. Zhang, *Appl. Phys. Lett.* **94**, 231912 (2009)
- [16] Z. Xu, M. J. Buechler, *ACS Nano* **4**, 3869 (2010).
- [17] M. Neek-Amal, F. M. Peeters, *Phys. Rev. B* **82**, 085432 (2010).
- [18] M. Neek-Amal, F. M. Peeters, *Appl. Phys. Lett.* **97**, 153118 (2010).
- [19] X. Tan, J. Wu, K. Zhang, X. Peng, L. Sun, J. Zhong, *Appl. Phys. Lett.* **102**, 071908 (2013).
- [20] Z. Qi, D. A. Bahamon, V. M. Pereira, H. S. Park, D. K. Campbell, A. H. Castro Neto, *Nano Lett.* **13**, 2692 (2013).
- [21] A. P. Sgouros, G. Kalosakas, M. M. Sigalas, K. Papagelis, *RSC Adv.* **5**, 39930 (2015).
- [22] E. N. Koukaras, G. Kalosakas, C. Galiotis, K. Papagelis, *Sci. Rep.* **5**, 12923 (2015).
- [23] A. P. Sgouros, G. Kalosakas, C. Galiotis, K. Papagelis, *2D Mater.* **3**, 025033 (2016).
- [24] J. Tersoff, *Phys. Rev. Lett.* **61**, 2879 (1988).
- [25] J. Tersoff, *Phys. Rev. B* **37**, 6991 (1988).
- [26] D. W. Brenner, *Phys. Rev. B* **42**, 9458 (1990).
- [27] L. Lindsay, D. A. Broido, *Phys. Rev. B* **81**, 205441 (2010).
- [28] J. H. Los, A. Fasolino, *Phys. Rev. B* **68**, 024107 (2003).
- [29] J. H. Los, L. M. Ghiringhelli, E. J. Meijer, A. Fasolino, *Phys. Rev. B* **72**, 214102 (2005).
- [30] S. J. Stuart, A. B. Tutein, J. A. Harrison, *J. Chem. Phys.* **112**, 6472 (2000).
- [31] D. Wei, Y. Song, and F. Wang, *J. Chem. Phys.* **134**, 184704 (2011).
- [32] Z. G. Fthenakis, G. Kalosakas, G. D. Chatzidakis, C. Galiotis, K. Papagelis, N. N. Lathiotakis, preprint (2017).
- [33] P. Giannozzi et al, *J. Phys.: Cond. Matt.* **21**, 395502 (2009).
- [34] A. Dal Corso, <http://www.quantum-espresso.org/wp-content/uploads>